

Magnetism and weak electronic correlations in Kagome metal ScV_6Sn_6

Tianye Yu,¹ Junwen Lai,^{1,2} Xiangyang Liu,^{1,2} Peitao Liu,¹ Xing-Qiu Chen,^{1,*} and Yan Sun^{1,†}

¹*Shenyang National Laboratory for Materials Science, Institute of Metal Research,
Chinese Academy of Sciences, Shenyang 110016, China.*

²*School of Materials Science and Engineering, University of Science and Technology of China, Shenyang 110016, China.*

As one class of typical quantum materials, Kagome metals in $AV_3\text{Sb}_5$ ($A = \text{K}, \text{Rb}, \text{Cs}$) have attracted extensive attentions due to their interesting physical properties and different quantum phases of charge density wave (CDW), superconductivity and nontrivial topology. Recently, a new CDW phase in ScV_6Sn_6 was experimentally observed and inspired a wide study of the mechanism of driving force. To have a clear understanding of the correlation effect in the CDW phase in ScV_6Sn_6 , we performed a systematic density functional theory plus dynamical mean field theory (DFT + DMFT) calculations. The resulting static local spin susceptibility is nearly independent of temperature, indicating the absence of local moment on atom V, in full agreement with experimental measurements. The mass enhancements of quasiparticles and bandwidth renormalizations near the Fermi level show a weak correlation strength in ScV_6Sn_6 . In addition, the comparable mass enhancements of quasiparticles in ScV_6Sn_6 with CDW order and YV_6Sn_6 without CDW phase suggests that electronic correlations corresponding to Fermi surface nesting do not play the dominant role in the formation of CDW order in ScV_6Sn_6 .

I. INTRODUCTION

Kagome lattice has received significant attention in last decades due to its fundamental symmetry and physics, which often present as linear band crossing, saddle point, and flat band, etc[1–8]. In recent years, much effort has been devoted to the study of these characteristic features present by Kagome lattice in real materials and impressive progresses have been made in this direction. For example, linear band crossings and flat bands in paramagnetic CoSn [9, 10] and antiferromagnetic FeSn [11, 12], and saddle points generated van Hove singularity in antiferromagnetic YMn_6Sn_6 [13] and paramagnetic GdV_6Sn_6 [14]. These realistic materials provide practical platforms for the study of the novel quantum phases, such as the anomalous Hall effect, topological band structure, flat bands, as well as fractional quantum Hall effect, etc.

In addition, some other interesting properties were found in Kagome metals. A series of Kagome metals in $AV_3\text{Sb}_5$ ($A = \text{K}, \text{Rb}, \text{Cs}$) were discovered to exhibit superconductivity at low temperatures ranging from 0.9 to 2.5 K [15–17]. Moreover, charge density wave (CDW) transitions at temperatures between 80 and 100 K were also observed in these systems[15–22], and van Hove singularity was believed to be one of the most important pre-requirements [23–34]. Very recently, a long-range CDW order of $\mathbf{q}_{CDW} = (1/3, 1/3, 1/3)$ was observed in ScV_6Sn_6 below 92 K, where the Kagome lattice constituted of atoms V [37], the same as $AV_3\text{Sb}_5$ ($A = \text{K}, \text{Rb}, \text{Cs}$). However, the CDW order in ScV_6Sn_6 is mainly caused by the out-plane charge density modulation [37], which contrasts with $AV_3\text{Sb}_5$ ($A = \text{K}, \text{Rb}, \text{Cs}$) but coincide with FeGe. To date, several theoretical framework to explore

the origin of the CDW order in ScV_6Sn_6 . According to current understanding, Fermi surface nesting (FSN) was ruled out by density functional theory (DFT) calculations [38, 39] and a giant q -dependent electron-phonon coupling has been proposed as an underlying mechanism [40]. However, it is important to consider another possible reason for electronic correlations arising from $3d$ orbitals in the atoms V that were not taken into account. Therefore, to achieve a comprehensive understanding, it is necessary to investigate the effect of electronic correlations, particularly in the formation of CDW order in ScV_6Sn_6 .

In this work, we carried out a systematic study on ScV_6Sn_6 by using density functional theory plus dynamical mean field theory (DFT + DMFT) method. The calculated dependence of static spin susceptibility on temperature indicates the absence of local moment on atom V and we attribute it to the strong hybridization between V $3d$ orbital and Sn $5p$, Sc $3d$ orbitals. The calculated mass enhancement m^*/m_{DFT} is about 1.3 and insensitive to the variation of temperature, similar to that in $AV_3\text{Sb}_5$ ($A = \text{K}, \text{Rb}, \text{Cs}$) [41, 42]. Meanwhile, there are some weak variations in band structure near the Fermi level (E_F) brought by electronic correlations. Hence, ScV_6Sn_6 is recognized as a weakly correlated metal. Furthermore, the Fermi surface is slightly affected by electronic correlations, validating the conclusion that FSN is not the driving force of CDW order in ScV_6Sn_6 drawn by previous DFT calculations [38–40]. We also compared the mass enhancements in ScV_6Sn_6 and YV_6Sn_6 where no CDW order was observed. The comparable values suggest that electronic correlations are not crucial for determining the CDW order in ScV_6Sn_6 .

* xingqiu.chen@imr.ac.cn

† sunyan@imr.ac.cn

II. METHODS

We conducted fully charge self-consistent DFT + DMFT calculations by using the eDMFT code [43] developed by Haule *et al.* The DFT part employed the linearized augmented plane-wave method as implemented in the WIEN2K package [44]. The Perdew-Burke-Ernzerhof generalized gradient approximation [45] was utilized for the exchange-correlation functional. Brillouin-zone integrations were performed on a $21 \times 21 \times 10$ mesh. The atomic sphere radii (R_{MT}) for Sc, V, and Sn were all set to 2.50 Bohr, and the plane-wave cutoff (K_{max}) was determined by $R_{\text{MT}} \times K_{\text{max}} = 7.0$. In the DMFT calculations, the projector to the local Green's function was fixed to the solution of the Dirac equation at the DFT level. Hybridization functions were considered within an energy window of 20 eV centered around E_F . We deal with the double counting by the formula of $U(n - 1/2) - J_H(n - 1)/2$, where $n = 3.0$ represents the nominal occupation of V $3d$ electrons, $U=5.0$ eV represents the Coulomb interaction parameter, and $J_H=0.7$ eV represents the Hund's exchange parameter. The adopted values are consistent with previous calculations in V-based correlated compounds, including AV_3Sb_5 ($A = \text{K, Rb, Cs}$) [41, 42] and vanadium oxides including SrVO_3 [46, 47], CaVO_3 [48], VO_2 [49] and V_2O_3 [50, 51]. For the DMFT impurity solver, we adopted the density-density form of Coulomb repulsion, which significantly accelerated the calculations. All five V $3d$ orbitals were treated as correlated. The DMFT quantum impurity problem was solved using the continuous-time quantum Monte Carlo (CTQMC) method [52, 53] at a temperature of $T = 116$ K. Upon achieving the desired accuracy, analytical continuation was performed using the maximum entropy method [43] to obtain the self-energy on the real axis and subsequently calculate the electronic structure. We have confirmed that the incorporation of spin-orbit coupling has negligible influence on the conclusion. We therefore only present the results without considering spin-orbit coupling in the following.

III. RESULTS AND DISCUSSION

A. Crystal structure

Figure 1(a) is the three-dimensional crystal structure of ScV_6Sn_6 , showing a typical HfFe_6Ge_6 -type compound. Within one unit cell of ScV_6Sn_6 , there are two Kagome layers formed by V and Sn2 atoms, one honeycomb layer formed by Sn3 atoms and one triangular layer formed by Sc and Sn1 atoms, see Fig. 1(b). Within each Kagome layer, Sn2 atoms are slightly off the plane formed by V atoms. The lattice constants and internal coordinates used in our calculations are optimized by the Vienna *Ab initio* Simulation Package (VASP) [54], until the atomic forces become less than 10^{-3} eV/Å. The obtained lattice constants and internal atomic coordinates

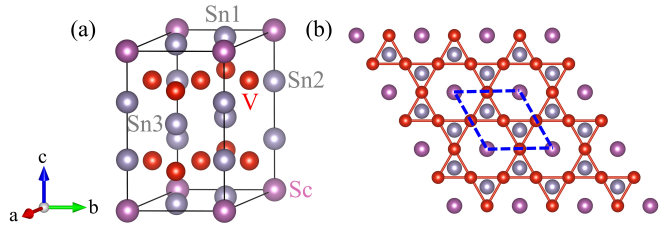


FIG. 1. (a) Crystal structure of ScV_6Sn_6 with space group $P6/mmm$ (No. 191). The gray, red, and pink atoms present atoms Sn, V, and Sc, respectively. (b) Top view along the c axis. Blue lines denote the unit cell of ScV_6Sn_6 .

are given in Table I, which are in good agreement with experimental reports [37] and previous calculations [38].

B. Magnetism

To investigate the magnetism of ScV_6Sn_6 and compare our calculational results with available experimental results, we present the temperature dependent static local spin susceptibility in Fig. 2(a). The static local spin susceptibility from CTQMC approach is defined as $\chi = \int_0^\beta \langle S_z(\tau) S_z(0) \rangle d\tau$, here β is the inverse temperature and τ is the imaginary time. We take temperatures ranging from 58 to 900 K in the paramagnetic state in the calculations. In a magnetic system with local moments, this value would show a T dependence, typically following the Curie-Weiss law. However, as presented by the red dots in Fig. 2(a), the susceptibility exhibits a paramagnetism with an almost flat line independence of T . For good metals, this behavior indicates the dominance of a Pauli paramagnetic response from itinerant electrons and the absence of local moments. This paramagnetic behavior resembles another V-based Kagome metal KV_3Sb_5 [42], as shown by the blue line in Fig. 2(a). The DFT + DMFT results here is consistent with recent experimental measurement [37].

To have more insight, we present the probability distribution for the different atomic configurations of V $3d$ shell in Fig. 2(b). Within the DFT + DMFT scheme, each V impurity has 1024 $3d$ states. The atomic histogram refers to the probability of finding a V impurity in each atomic state. We note that only those states oc-

TABLE I. The relaxed internal atomic coordinates in ScV_6Sn_6 with the lattice constants $a = b = 5.454$ Å, and $c = 9.230$ Å.

Atom	Wyckoff position	x	y	z
Sc	1a	0	0	0
V	6i	1/2	0	0.248
Sn1	2c	1/3	2/3	0
Sn2	2e	0	0	0.320
Sn3	2d	1/3	2/3	1/2

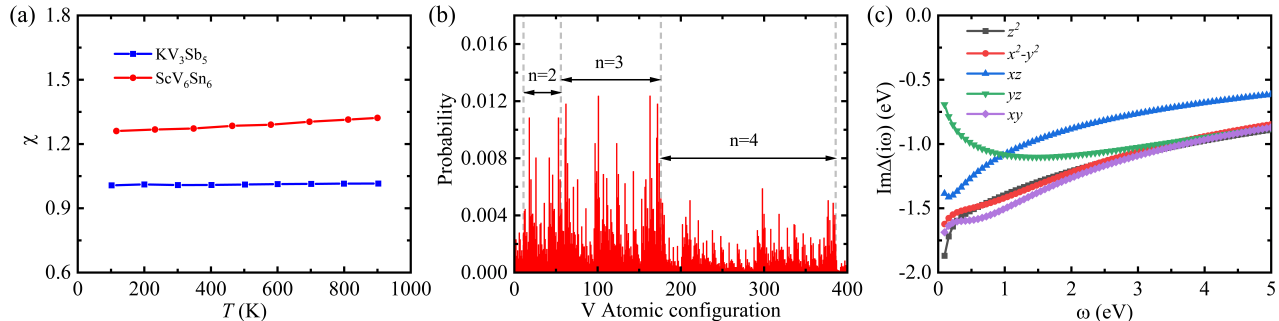


FIG. 2. (a) Temperature dependent spin susceptibility obtained from CTQMC. The blue and red dots are ScV_6Sn_6 and KV_3Sb_5 , respectively. The values of spin susceptibility of KV_3Sb_5 are from reference [42]. (b) Density functional theory (DFT) + dynamical mean field theory (DMFT) calculated atomic histogram of V $3d$ orbitals in ScV_6Sn_6 , with $U = 5$ eV and $J_H = 0.7$ eV. The states with occupation number exceeding five are not shown due to their negligible probabilities. (c) Imaginary part of the hybridization function on Matsubara frequencies at $T = 116$ K.

cupied by $N = 2, 3,$ and 4 electrons have considerable probabilities. Hence the states with larger orbital occupation number ($N > 5$) are not presented in Fig. 2(b). For the states with the same occupation number N , we arrange the states in descending order in accordance with their $|S_z|$ values. Note that in the atomic limit, the configuration with occupancy $n_d = 3$ should typically favor the high-spin state according to the Hund's rule. However, this is not the case in Fig. 2(b). Here, the close competition between different occupancy and spin states indicates strong charge and spin fluctuations in paramagnetic ScV_6Sn_6 . This can be attributed to the strong hybridization between V $3d$, Sn $5p$, and Sc $3d$ orbitals. Figure 2(c) presents the imaginary parts of hybridization functions of the V $3d$ orbitals, which indicate a substantial delocalization of these orbitals (larger than 0.5 eV), especially for V- d_{z^2} orbital.

C. Mass enhancement

The effective mass enhancement is a straightforward and quantitative way to characterize the strength of electronic correlations. For weakly correlated systems, it is almost equal to 1 but much greater than 1 in strongly correlated systems, such as iron-based superconductors [55] and heavy fermion materials [56, 57]. Within the DFT + DMFT method, we can obtain the effective mass enhancement m^*/m_{DFT} , which is equal to $1/Z$, and Z is the quasiparticle weight $Z = 1/(1 - \frac{\partial \text{Im}\Sigma(i\omega_n)}{\partial \omega_n}|_{\omega_n \rightarrow 0})$, according to the calculated self-energy on Matsubara frequencies.

Figure 3(a) presents the imaginary parts of self-energy for all five V $3d$ orbitals at the temperature of 116 K in the paramagnetic state. In practice, we obtain m^*/m_{DFT} for each V $3d$ orbital by average the values computed by origin and the lowest Matsubara point and the lowest two Matsubara points. Figure 3(b) displays the computed mass enhancement m^*/m_{DFT} in ScV_6Sn_6 with different values of Coulomb interaction U ranging from 3 to 7 eV and Hund interaction $J_H = 0.14 \times U$. For a typical U of 5.0 eV and J_H of 0.7 eV that is commonly used for other V-based compounds [41, 42, 46–51], our computed values of m^*/m_{DFT} in ScV_6Sn_6 at 116 K are 1.406, 1.266, 1.345, 1.265, and 1.369 for V- d_{z^2} , V- $d_{x^2-y^2}$, V- d_{xz} , V- d_{yz} , and V- d_{xy} orbitals, respectively. These values are significantly smaller than the typical values in strongly correlated systems, suggesting the weak correlations in this compound. As shown in Figure 3(b), the V- d_{z^2} orbital emerges as the most responsive to changes in the interaction parameters. However, despite setting the value of U to 7 eV, the mass enhancement of V- d_{z^2} orbital only reaches a maximum value of 1.850. Furthermore, it has been confirmed that the computed value of m^*/m_{DFT} shows a small variation with temperature. For instance, the calculated m^*/m_{DFT} of V- d_{z^2} is 1.421 at 58 K and 1.400 at 232 K.

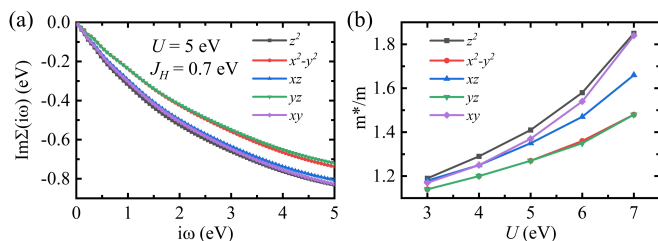


FIG. 3. (a) Imaginary part of the self-energy of V $3d$ shell on Matsubara frequencies at $T = 116$ K. (b) The mass enhancement m^*/m_{DFT} in ScV_6Sn_6 with different combinations of Coulomb interaction U and J_H (for each value of U , J_H is equal to $0.14 \times U$).

D. Correlated electronic structure

To investigate the effect of electronic correlations on electronic structure of ScV_6Sn_6 , we firstly plot the energy dispersion and density of states (DOS) calculated by DFT in Fig. 4(a). There is a large peak in DOS around 0.3 eV above E_F with a V $3d$ character, which could be attributed to the flat band along the Γ - M - K - Γ path, a typical feature present by Kagome lattice. From the band structure, we observe that this flat band is mainly contributed by V - d_{z^2} orbital. Another two characteristics of Kagome lattice can also be seen, including linear band crossings at K and saddle points at M just below E_F , in agreement with previous studies [38, 40].

As a comparison, we plot the momentum-resolved spectral functions and momentum-integrated spectral functions obtained by the DFT + DMFT method in Fig. 4(b). The most obvious feature of the momentum-resolved spectral functions is the incoherence away from E_F , indicating a somewhat short quasiparticle lifetime away from E_F . However, the spectra near E_F exhibit good coherence, and the bandwidths are weakly renormalized when compared with the DFT band structure represented by the gold dashed lines. Overall, our calculations show that ScV_6Sn_6 could be a weakly correlated metal. It is necessary to emphasize that while local correlation is adequately considered in the DFT + DMFT calculation, the influence of long-range correlation on the electronic structure of ScV_6Sn_6 has been omitted. Therefore, it is imperative to investigate the impact of long-range correlation in future research. For instance, employing the DFT + HSE06 method would provide valuable insights into this aspect.

Figure 5(a) shows the DFT Fermi surface in the first Brillouin zone. In contrast to $AV_3\text{Sb}_5$ ($A = \text{K, Rb, Cs}$) [41, 42], one prominent distinguishing feature is the three-dimensionality with respect to k_z . Comparing the Fermi surfaces from DFT and DFT + DMFT, one can see that the most obvious variation brought by electronic correlations are the increment of the size of the pocket centered at the middle of $L - M$, see Fig. 5(b). This variation could be due to the lift of the bands forming a crossing near E_F along $L - M$. However, apart from this discrepancy, the Fermi surface obtained by the DFT + DMFT method is quite similar to that from DFT.

E. Charge density wave

FSN is one of the underlying mechanisms of the lattice instability. The idea is that if Fermi surface contours coincide when shifted along the observed CDW wave vector, then the CDW is considered to be nesting derived. The imaginary part of the bare charge susceptibility under zero-frequency limit, namely FSN function, describing the degree of the FSN with a certain nesting vector q is defined as $\lim_{\omega \rightarrow 0} \chi''_0(\mathbf{q}, \omega)/\omega =$

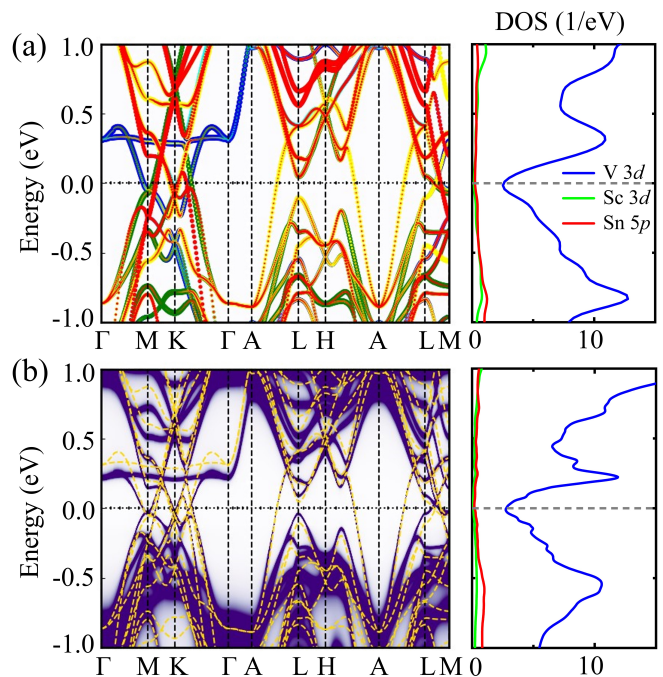


FIG. 4. (a) Orbital projected DFT energy dispersion and density of states, with V - d_{z^2} , V - $d_{x^2-y^2}$, V - d_{xy} , V - d_{xz} and V - d_{yz} orbitals labeled by blue, cyan, green, yellow and red lines, respectively. (b) Momentum-resolved spectral functions and momentum-integrated spectral functions from DFT + DMFT method at $T = 116$ K. The DFT band structure given by gold dashed lines is attached for comparison.

$\sum_{nn', \mathbf{k}} \delta(\epsilon_{n, \mathbf{k}} - \epsilon_0) \delta(\epsilon_{n', \mathbf{k}+\mathbf{q}} - \epsilon_0)$ where δ is the Dirac-delta function, $\epsilon_{n, \mathbf{k}}$ is the eigenvalue of n th band at \mathbf{k} point, and ϵ_0 is the Fermi energy.

FSN was revealed as a strong candidate for driving CDW formation in rare-earth tritellurides, including GdTe_3 and LuTe_3 [58]. However, according to previous DFT calculations, FSN was excluded as the primary driving force behind the CDW order in ScV_6Sn_6 [38, 39]. To take electronic correlations into account, we plot the DFT + DMFT calculated FSN function on the $q_z = 0, 1/3,$ and $1/2$ planes, respectively, in Fig. 6. Here a dense \mathbf{k} -mesh of $100 \times 100 \times 51$ and a small Gaussian broadening factor of 0.001 eV in Dirac-delta functions are used to display

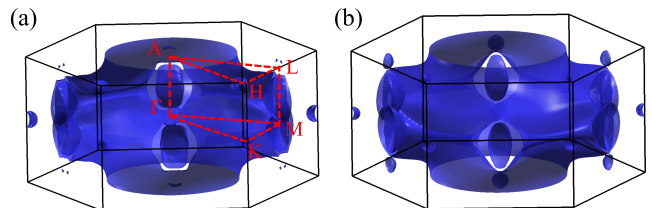


FIG. 5. (a) DFT and (b) DFT + DMFT calculated Fermi surfaces of ScV_6Sn_6 in the first Brillouin zone.

TABLE II. DFT + DMFT calculated orbital occupation of V $3d$ orbitals and mass enhancement obtained from the quasiparticle self-energy.

	Orbital occupation					Mass enhancement				
	d_{z^2}	$d_{x^2-y^2}$	d_{xz}	d_{yz}	d_{xy}	d_{z^2}	$d_{x^2-y^2}$	d_{xz}	d_{yz}	d_{xy}
ScV ₆ Sn ₆	0.803	0.512	0.569	0.454	0.924	1.406	1.266	1.345	1.265	1.369
YV ₆ Sn ₆	0.790	0.500	0.590	0.459	0.906	1.423	1.275	1.368	1.271	1.393

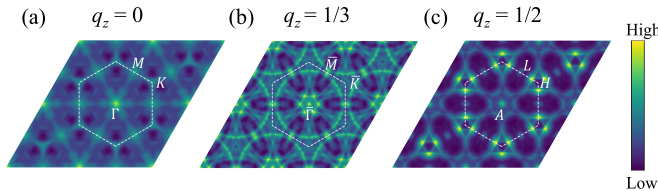


FIG. 6. The DFT + DMFT calculated imaginary parts of the electron susceptibility $\chi(q)$, namely Fermi surface nesting function, on (a) $q_z = 0$, (b) $q_z = 1/3$ and (c) $q_z = 1/2$ planes. White hexagons in all panels represent the in-plane Brillouin zone, corresponding high-symmetry points on each plane are labeled.

the relative strength of the FSN function at different q points. In contrast to AV_3Sb_5 ($A = K, Rb, Cs$) with weak q_z dependence [41, 42], the maximum of the FSN function of ScV₆Sn₆ undergoes a transition. Specifically, as q_z varies from 0 to $1/3$ to $1/2$, the maximum shifts from M (Fig. 6(a)) to along $\Gamma - M$ and near Γ (Fig. 6(b)), and ultimately settles at the middle of $L - H$ (Fig. 6(c)). Single crystal x-ray diffraction determined CDW wave vector in ScV₆Sn₆ is $\mathbf{q}_{CDW} = (1/3, 1/3, 1/3)$ [37]. If the CDW is indeed caused by FSN, the maximum should be located at the \bar{K} point in Fig. 6(b), but this is not the case. We therefore conclude that FSN is unlikely to be the direct cause of the CDW instability in ScV₆Sn₆ even when electronic correlations are considered.

To further illustrate the dependence of CDW order on electronic correlations, we compare the correlation strength of quasiparticles in ScV₆Sn₆ and non-CDW compound YV₆Sn₆. Owing to the larger radius of atom Y, lattice constant a is larger in YV₆Sn₆ than ScV₆Sn₆ [59]. However, as listed in Table II, the calculated orbital occupation numbers and mass enhancements in these two compounds exhibit a striking similarity. For instance, the mass enhancement of the most correlated orbital $V-d_{z^2}$ is 1.406 in ScV₆Sn₆ and 1.423 in YV₆Sn₆. We propose that electronic correlations are not crucial for the formation of CDW order in ScV₆Sn₆.

Recently, Cao *et al.* [40] observed a remarkably large

q -dependent electron-phonon coupling, which has been proposed as the underlying mechanism responsible for the CDW order in ScV₆Sn₆. Given the weak electronic correlation strength observed in our DFT + DMFT calculations, the electronic correlations will not significantly affect this conclusion. Therefore, we support the notion that the q -dependent electron-phonon coupling is a strong candidate for driving the CDW order in ScV₆Sn₆.

IV. CONCLUSIONS

In summary, based on DFT + DMFT calculations, we studied the magnetism and electronic correlation effects in ScV₆Sn₆. The spin susceptibility is nearly independent of temperature, indicating the absence of local moment on atom V and consistent with experimental reports. By analyzing the computed atomic histogram and hybridization functions, we attribute the absence of local moment to the strong hybridization between V $3d$, Sn $5p$, and Sc $3d$ orbitals. The mass enhancement is about 1.3 and the bandwidths near E_F are weakly renormalized by electronic correlations, indicating the weak electronic correlation strength in ScV₆Sn₆. The calculated FSN function with the inclusion of electronic correlations shows no maximum at experimentally determined \mathbf{q}_{CDW} , suggesting that FSN is not the driving force of CDW order in ScV₆Sn₆. Furthermore, the comparable values of quasiparticle mass enhancements in ScV₆Sn₆ and non-CDW YV₆Sn₆ suggest that the electronic correlations play a non-crucial role in the formation of the CDW order in ScV₆Sn₆.

ACKNOWLEDGMENTS

This work was supported by the National Key R&D Program of China (Grant No. 2021YFB3501503) and the National Natural Science Foundation of China (Grants No. 52271016 and No. 52188101). Part of the numerical calculations in this study were carried out on the ORISE Supercomputer.

[1] J.-X. Yin, B. Lian, and M. Z. Hasan, Topological kagome magnets and superconductors, *Nature* **612**, 647 (2022).

[2] L. Ye, M. Kang, J. Liu, F. Von Cube, C. R. Wicker, T. Suzuki, C. Jozwiak, A. Bostwick, E. Rotenberg, D. C. Bell, *et al.*, Massive dirac fermions in a ferromagnetic

- kagome metal, *Nature* **555**, 638 (2018).
- [3] A. Nag, Y. Peng, J. Li, S. Agrestini, H. Robarts, M. García-Fernández, A. Walters, Q. Wang, Q. Yin, H. Lei, *et al.*, Correlation driven near-flat band stoner excitations in a kagome magnet, *Nature Communications* **13**, 7317 (2022).
 - [4] T. Yu, R. Liu, Y. Peng, P. Zheng, G. Wang, X. Ma, Z. Yuan, and Z. Yin, Correlated electronic structure of the kagome metal Mn_3Sn , *Physical Review B* **106**, 205103 (2022).
 - [5] C. Mielke III, D. Das, J.-X. Yin, H. Liu, R. Gupta, Y.-X. Jiang, M. Medarde, X. Wu, H. C. Lei, J. Chang, *et al.*, Time-reversal symmetry-breaking charge order in a kagome superconductor, *Nature* **602**, 245 (2022).
 - [6] H. Chen, H. Yang, B. Hu, Z. Zhao, J. Yuan, Y. Xing, G. Qian, Z. Huang, G. Li, Y. Ye, *et al.*, Roton pair density wave in a strong-coupling kagome superconductor, *Nature* **599**, 222 (2021).
 - [7] H.-M. Guo and M. Franz, Topological insulator on the kagome lattice, *Physical Review B* **80**, 113102 (2009).
 - [8] N. J. Ghimire and I. I. Mazin, Topology and correlations on the kagome lattice, *Nature Materials* **19**, 137 (2020).
 - [9] M. Kang, S. Fang, L. Ye, H. C. Po, J. Denlinger, C. Jozwiak, A. Bostwick, E. Rotenberg, E. Kaxiras, J. G. Checkelsky, *et al.*, Topological flat bands in frustrated kagome lattice cosn, *Nature communications* **11**, 4004 (2020).
 - [10] Z. Liu, M. Li, Q. Wang, G. Wang, C. Wen, K. Jiang, X. Lu, S. Yan, Y. Huang, D. Shen, *et al.*, Orbital-selective dirac fermions and extremely flat bands in frustrated kagome-lattice metal cosn, *Nature communications* **11**, 4002 (2020).
 - [11] M. Kang, L. Ye, S. Fang, J.-S. You, A. Levitan, M. Han, J. I. Facio, C. Jozwiak, A. Bostwick, E. Rotenberg, *et al.*, Dirac fermions and flat bands in the ideal kagome metal fesn, *Nature materials* **19**, 163 (2020).
 - [12] M. Han, H. Inoue, S. Fang, C. John, L. Ye, M. K. Chan, D. Graf, T. Suzuki, M. P. Ghimire, W. J. Cho, *et al.*, Evidence of two-dimensional flat band at the surface of antiferromagnetic kagome metal fesn, *Nature communications* **12**, 5345 (2021).
 - [13] M. Li, Q. Wang, G. Wang, Z. Yuan, W. Song, R. Lou, Z. Liu, Y. Huang, Z. Liu, H. Lei, *et al.*, Dirac cone, flat band and saddle point in kagome magnet YMn_6Sn_6 , *Nature communications* **12**, 3129 (2021).
 - [14] S. Peng, Y. Han, G. Pokharel, J. Shen, Z. Li, M. Hashimoto, D. Lu, B. R. Ortiz, Y. Luo, H. Li, *et al.*, Realizing Kagome Band Structure in Two-Dimensional Kagome Surface States of RV_6Sn_6 (R= Gd, Ho), *Physical review letters* **127**, 266401 (2021).
 - [15] B. R. Ortiz, P. M. Sarte, E. M. Kenney, M. J. Graf, S. M. Teicher, R. Seshadri, and S. D. Wilson, Superconductivity in the Z_2 kagome metal KV_3Sb_5 , *Physical Review Materials* **5**, 034801 (2021).
 - [16] Q. Yin, Z. Tu, C. Gong, Y. Fu, S. Yan, and H. Lei, Superconductivity and normal-state properties of kagome metal RbV_3Sb_5 single crystals, *Chinese Physics Letters* **38**, 037403 (2021).
 - [17] B. R. Ortiz, S. M. Teicher, Y. Hu, J. L. Zuo, P. M. Sarte, E. C. Schueller, A. M. Abeykoon, M. J. Krogstad, S. Rosenkranz, R. Osborn, *et al.*, CsV_3Sb_5 : A Z_2 topological kagome metal with a superconducting ground state, *Physical Review Letters* **125**, 247002 (2020).
 - [18] B. R. Ortiz, L. C. Gomes, J. R. Morey, M. Winiarski, M. Bordelon, J. S. Mangum, I. W. Oswald, J. A. Rodriguez-Rivera, J. R. Neilson, S. D. Wilson, *et al.*, New kagome prototype materials: discovery of KV_3Sb_5 , RbV_3Sb_5 , and CsV_3Sb_5 , *Physical Review Materials* **3**, 094407 (2019).
 - [19] Y.-X. Jiang, J.-X. Yin, M. M. Denner, N. Shumiya, B. R. Ortiz, G. Xu, Z. Guguchia, J. He, M. S. Hossain, X. Liu, *et al.*, Unconventional chiral charge order in kagome superconductor KV_3Sb_5 , *Nature materials* **20**, 1353 (2021).
 - [20] H. Li, T. Zhang, T. Yilmaz, Y. Pai, C. Marvinney, A. Said, Q. Yin, C. Gong, Z. Tu, E. Vescovo, *et al.*, Observation of Unconventional Charge Density Wave without Acoustic Phonon Anomaly in Kagome Superconductors AV_3Sb_5 (A= Rb, Cs), *Physical Review X* **11**, 031050 (2021).
 - [21] Z. Liang, X. Hou, F. Zhang, W. Ma, P. Wu, Z. Zhang, F. Yu, J.-J. Ying, K. Jiang, L. Shan, *et al.*, Three-dimensional charge density wave and surface-dependent vortex-core states in a kagome superconductor CsV_3Sb_5 , *Physical Review X* **11**, 031026 (2021).
 - [22] H. Tan, Y. Liu, Z. Wang, and B. Yan, Charge density waves and electronic properties of superconducting kagome metals, *Physical review letters* **127**, 046401 (2021).
 - [23] X. Feng, K. Jiang, Z. Wang, and J. Hu, Chiral flux phase in the Kagome superconductor AV_3Sb_5 , *Science bulletin* **66**, 1384 (2021).
 - [24] M. L. Kiesel, C. Platt, and R. Thomale, Unconventional fermi surface instabilities in the kagome hubbard model, *Physical review letters* **110**, 126405 (2013).
 - [25] K. Jiang, T. Wu, J.-X. Yin, Z. Wang, M. Z. Hasan, S. D. Wilson, X. Chen, and J. Hu, Kagome superconductors AV_3Sb_5 (A= K, Rb, Cs), *National Science Review* **10**, nwac199 (2023).
 - [26] L. Nie, K. Sun, W. Ma, D. Song, L. Zheng, Z. Liang, P. Wu, F. Yu, J. Li, M. Shan, *et al.*, Charge-density-wave-driven electronic nematicity in a kagome superconductor, *Nature* **604**, 59 (2022).
 - [27] W.-S. Wang, Z.-Z. Li, Y.-Y. Xiang, and Q.-H. Wang, Competing electronic orders on kagome lattices at van Hove filling, *Physical Review B* **87**, 115135 (2013).
 - [28] H. Tan, Y. Liu, Z. Wang, and B. Yan, Charge density waves and electronic properties of superconducting kagome metals, *Physical review letters* **127**, 046401 (2021).
 - [29] M. M. Denner, R. Thomale, and T. Neupert, Analysis of Charge Order in the Kagome Metal AV_3Sb_5 (A= K, Rb, Cs), *Physical Review Letters* **127**, 217601 (2021).
 - [30] Y.-P. Lin and R. M. Nandkishore, Complex charge density waves at Van Hove singularity on hexagonal lattices: Haldane-model phase diagram and potential realization in the kagome metals AV_3Sb_5 (A= K, Rb, Cs), *Physical Review B* **104**, 045122 (2021).
 - [31] T. Park, M. Ye, and L. Balents, Electronic instabilities of kagome metals: saddle points and landau theory, *Physical Review B* **104**, 035142 (2021).
 - [32] M. H. Christensen, T. Birol, B. M. Andersen, and R. M. Fernandes, Theory of the charge density wave in AV_3Sb_5 kagome metals, *Physical Review B* **104**, 214513 (2021).
 - [33] H. Zhao, H. Li, B. R. Ortiz, S. M. Teicher, T. Park, M. Ye, Z. Wang, L. Balents, S. D. Wilson, and I. Zeljkovic, Cascade of correlated electron states in the kagome superconductor CsV_3Sb_5 , *Nature* **599**, 216

- (2021).
- [34] H. Li, T. Zhang, T. Yilmaz, Y. Pai, C. Marvinney, A. Said, Q. Yin, C. Gong, Z. Tu, E. Vescovo, *et al.*, Observation of Unconventional Charge Density Wave without Acoustic Phonon Anomaly in Kagome Superconductors AV_3Sb_5 ($A = Rb, Cs$), *Physical Review X* **11**, 031050 (2021).
- [35] X. Teng, L. Chen, F. Ye, E. Rosenberg, Z. Liu, J.-X. Yin, Y.-X. Jiang, J. S. Oh, M. Z. Hasan, K. J. Neubauer, *et al.*, Discovery of charge density wave in a kagome lattice antiferromagnet, *Nature* **609**, 490 (2022).
- [36] Y. Wang, Enhanced spin-polarization via partial g-dimerization as the driving force of the charge density wave in fege, *Physical Review Materials* **7**, 104006 (2023).
- [37] H. W. S. Arachchige, W. R. Meier, M. Marshall, T. Matsuoka, R. Xue, M. A. McGuire, R. P. Hermann, H. Cao, and D. Mandrus, Charge Density Wave in Kagome Lattice Intermetallic ScV_6Sn_6 , *Physical Review Letters* **129**, 216402 (2022).
- [38] H. Tan and B. Yan, Abundant Lattice Instability in Kagome Metal ScV_6Sn_6 , *Physical review letters* **130**, 266402 (2023).
- [39] T. Hu, H. Pi, S. Xu, L. Yue, Q. Wu, Q. Liu, S. Zhang, R. Li, X. Zhou, J. Yuan, *et al.*, Optical spectroscopy and band structure calculations of the structural phase transition in the vanadium-based kagome metal ScV_6Sn_6 , *Physical Review B* **107**, 165119 (2023).
- [40] S. Cao, C. Xu, H. Fukui, T. Manjo, M. Shi, Y. Liu, C. Cao, and Y. Song, Competing charge-density wave instabilities in the kagome metal ScV_6Sn_6 , *arXiv preprint arXiv:2304.08197* (2023).
- [41] M. Liu, Z. Wang, and J.-J. Zhou, Weak electronic correlations in the kagome superconductor AV_3Sb_5 ($A = K, Rb, Cs$), *Physical Review B* **105**, 235130 (2022).
- [42] J. Zhao, W. Wu, Y. Wang, and S. A. Yang, Electronic correlations in the normal state of the kagome superconductor KV_3Sb_5 , *Physical Review B* **103**, L241117 (2021).
- [43] K. Haule, C.-H. Yee, and K. Kim, Dynamical mean-field theory within the full-potential methods: Electronic structure of $CeIrIn_5$, $CeCoIn_5$, and $CeRhIn_5$, *Physical Review B* **81**, 195107 (2010).
- [44] P. Blaha, K. Schwarz, G. K. Madsen, D. Kvasnicka, J. Luitz, *et al.*, wien2k, An augmented plane wave+local orbitals program for calculating crystal properties **60** (2001).
- [45] J. P. Perdew, K. Burke, and M. Ernzerhof, Generalized gradient approximation made simple, *Physical review letters* **77**, 3865 (1996).
- [46] E. Pavarini, S. Biermann, A. Poteryaev, A. Lichtenstein, A. Georges, and O. Andersen, Mott transition and suppression of orbital fluctuations in orthorhombic $3d^1$ perovskites, *Physical review letters* **92**, 176403 (2004).
- [47] C. Taranto, M. Kaltak, N. Parragh, G. Sangiovanni, G. Kresse, A. Toschi, and K. Held, Comparing quasiparticle GW+DMFT and LDA+DMFT for the test bed material $SrVO_3$, *Physical Review B* **88**, 165119 (2013).
- [48] I. A. Nekrasov, G. Keller, D. Kondakov, A. Kozhevnikov, T. Pruschke, K. Held, D. Vollhardt, and V. Anisimov, Comparative study of correlation effects in $CaVO_3$ and $SrVO_3$, *Physical Review B* **72**, 155106 (2005).
- [49] M. Laad, L. Craco, and E. Müller-Hartmann, Metal-insulator transition in rutile-based VO_2 , *Physical Review B* **73**, 195120 (2006).
- [50] K. Held, G. Keller, V. Eyert, D. Vollhardt, and V. I. Anisimov, Mott-Hubbard Metal-Insulator Transition in Paramagnetic V_2O_3 : An LDA+DMFT (QMC) Study, *Physical review letters* **86**, 5345 (2001).
- [51] K. Held, I. Nekrasov, G. Keller, V. Eyert, N. Blümer, A. McMahan, R. Scalettar, T. Pruschke, V. Anisimov, and D. Vollhardt, Realistic investigations of correlated electron systems with LDA+DMFT, *physica status solidi (b)* **243**, 2599 (2006).
- [52] P. Werner, A. Comanac, L. De'Medici, M. Troyer, and A. J. Millis, Continuous-time solver for quantum impurity models, *Physical Review Letters* **97**, 076405 (2006).
- [53] K. Haule, Quantum monte carlo impurity solver for cluster dynamical mean-field theory and electronic structure calculations with adjustable cluster base, *Physical Review B* **75**, 155113 (2007).
- [54] G. Kresse and J. Furthmüller, Efficient iterative schemes for ab initio total-energy calculations using a plane-wave basis set, *Physical review B* **54**, 11169 (1996).
- [55] Z. Yin, K. Haule, and G. Kotliar, Kinetic frustration and the nature of the magnetic and paramagnetic states in iron pnictides and iron chalcogenides, *Nature materials* **10**, 932 (2011).
- [56] H. C. Choi, E. D. Bauer, F. Ronning, and J.-X. Zhu, DFT+DMFT study of dopant effects in the heavy-fermion compound $CeCoIn_5$, *Physical Review B* **105**, 115121 (2022).
- [57] M. Liu, Y. Xu, D. Hu, Z. Fu, N. Tong, X. Chen, J. Cheng, W. Xie, and Y.-f. Yang, Symmetry-enforced heavy-fermion physics in the quadruple-perovskite $CaCu_3Ir_4O_{12}$, *arXiv preprint arXiv:1705.00846* (2017).
- [58] J. Laverock, S. Dugdale, Z. Major, M. Alam, N. Ru, I. Fisher, G. Santi, and E. Bruno, Fermi surface nesting and charge-density wave formation in rare-earth tritellurides, *Physical Review B* **71**, 085114 (2005).
- [59] L. Romaka, Y. Stadnyk, V. Romaka, P. Demchenko, M. Stadnyshyn, and M. Konyk, Peculiarities of component interaction in Gd, Er-V-Sn Ternary systems at 870 K and crystal structure of RV_6Sn_6 stannides, *Journal of alloys and compounds* **509**, 8862 (2011).